Biophysical Journal Volume 101 August 2011 1004–1013

Flow of Excitation Energy in the Cryptophyte Light-Harvesting Antenna Phycocyanin 645

Alessandro Marin,[†] Alexander B. Doust,[†‡§¶] Gregory D. Scholes,[‡§¶] Krystyna E. Wilk,[‖**] Paul M. G. Curmi,[‖**] Ivo H. M. van Stokkum,[†] and Rienk van Grondelle[†*]

[†]Faculty of Sciences, Vrije Universiteit Amsterdam, Amsterdam, The Netherlands; [‡]Department of Chemistry, [§]Institute for Optical Sciences, and [¶]Centre for Quantum Information and Quantum Control, University of Toronto, Toronto, Ontario, Canada; and [‖]School of Physics and **Centre for Applied Medical Research, St. Vincent's Hospital, University of New South Wales, Sydney, New South Wales, Australia

ABSTRACT We report a detailed description of the energy migration dynamics in the phycocyanin 645 (PC645) antenna complex from the photosynthetic alga *Chroomonas* CCMP270. Many of the cryptophyceae are known to populate greater depths than most other algal families, having developed a 99.5% efficient light-harvesting system. In this study, we used femtosecond time-resolved spectroscopy and global analysis to characterize the excited-state dynamics of PC645. Several different pump colors were selected to excite different fractions of the four phycobiliprotein pairs present in the complex. Measurements were also performed at cryogenic temperature to enhance spectral resolution and selectively promote downhill energy transfers. Upon excitation of the highest-energy bilins (dihydrobiliverdins), energy is transferred from the core of the complex to the periphery within 0.82 ps. Four bilins (mesobiliverdin (MBV) A/B and phycocyanobilins (PCB) 158C/D), which are responsible for the central band of the absorption spectrum, show concerted spectral dynamics. These chromophores show a biphasic decay with lifetimes of 0.6 ps (MBV) and 5–7 ps (PCB 158) to the lowest bilin pair (PCB 82C/D) absorbing around 650–657 nm. Within this lifetime of several picoseconds, the excitations reach the PCB 82 bilins on the two poles at the smaller sides of PC645. A slow 44–46 ps energy transfer step to the lowest-energy PCB 82 bilin concludes the dynamics.

INTRODUCTION

Cryptomonads constitute a group of unicellular eukaryotes that populate both marine and freshwater aquatic environments. These algae find their natural habitat below surface waters, possibly covered by other photosynthetic organisms. Most of these species are photosynthetic and are named cryptophytes. Cryptophytes are endowed with a chloroplast, which is the evolutionary result of ingestion of a red alga as an endosymbiont (1–3). As a consequence of their habitat, cryptophytes have adapted to absorb the low light available in the blue-green range of the spectrum filtered through the water column and to process photons with high efficiency (4). This capacity is achieved through two types of light-harvesting systems in the cryptophyte plastid: the Chlorophyll *a*/*c*2 complex inside the thylakoid membranes, and the light-harvesting phycobiliprotein systems stacked in the lumen (5,6). The interluminal antennae are organized as a quaternary $\alpha\alpha'\beta\beta$ heterodimeric structure (7,8). The different cryptophyte species differ in the composition of their phycobilins, which are open-chain tetrapyrroles covalently bound to the protein (9).

The pigment-protein structures of the cryptophyte species *Rhodomonas* CS24 and *Chroomonas* CCMP270 are known (8,10,11). The spectral properties of PC645 are determined by four bilin pairs, with six bilins located in the two symmetric β-subunits (dihydrobiliverdins 50/61 (DBV) and phycocyanobilins 158 and 82 (PCB 158 and 82), located on the C and D helixes, respectively) and two bilins located in the quasi-symmetric α/α' subunits (mesobiliverdins 19 A and B (MBV)).

Research on cryptophytes has been carried out since 1950 (for a review, see Hill and Rowan (12)), leading to the assessment that each species contains only a single type of phycobiliprotein. Experiments in the 1970s (13,14) grouped different types of chromophores depending on the absorption wavelength. In PC645, Kobayashi et al. (15) and Holzwarth et al. (16) found evidence for energy transfer between different pigment types by detecting several picosecond components in pump-probe and fluorescence experiments, which was discussed in the framework of Jung et al.'s (17) chromophore coupling model. Later, Malak and MacColl (18) studied PC645 with excitation at three wavelengths. An energy transfer model was proposed in which the 585 and 624 nm species lead independently to 650 nm emitting states in 2 and 15 ps, and a high-energy species transfers in 9 ps to the 585 nm species (18,19).

The discovery of the crystal structure of PC645 (11) enabled investigators to perform quantum chemical calculations to elucidate the spectral positions of single bilin molecules (11,20). Mirkovic et al. (20) reported that the chromophores that give rise to the highest-energy band in the absorption spectrum of PC645, at 585 nm, are the DBVs, which are characterized by strong mixing and an energy splitting of their eigenstates of about 640 cm^{-1}. The MBV pair at 610–622 nm and the four PCB bilins at

Submitted May 3, 2011, and accepted for publication July 14, 2011.

*Correspondence: r.van.grondelle@vu.nl

Alexander B. Doust's present address is Cambridge Display Technology, Cambridgeshire, United Kingdom.

Editor: Leonid S. Brown.

0006-3495/11/08/1004/10 $2.00

doi: 10.1016/j.bpj.2011.07.012

630 and 640 nm are next on the energy scale. PCB 82 is attributed to the lowest-energy bilins responsible for the fluorescence emission at 662 nm.

Mirkovic et al. (20) also used several spectroscopic methods to study PC645. Emission anisotropy provided evidence for one single emitting chromophore. The bands at 585 and 600 nm were assigned to the DBV and MBV, respectively. Single-wavelength, pump-probe anisotropy traces were recorded at 585, 620, 645, and 664 nm. It was inferred that excitation energy transfer (EET) from the high-energy species DBV to the MBV and to PCB takes place in 0.6 and 12 ps, respectively, followed by relaxation to the red PCB 82 states in ~10 ps. The slowest 15.5 ps decay of the 664 nm anisotropy traces was attributed to the final PCB 82D to PCB 82C EET process, in contrast to quantum chemical calculations that predicted an energy transfer time of 40 ps (20).

In a fluorescence study on PC645 and intact *Chroomonas* cells (4), a 2 ps component after 582 nm excitation was found to be due to fast relaxation within the complex. The energy transfer between the two terminal PCB bilins was estimated to lie in the 15–40 ps range, whereas a 45 ps component was found to describe the transfer from PC645 to the external Chlorophyll *a*/*c*2 complexes. Remarkably, in intact cells, only 0.5% of the excitations was lost as fluorescence, which was fitted with a 1.38 ns component, in agreement with previous studies (15,16,18).

Two-dimensional photon echo experiments (21) showed an anticorrelated behavior of the crosspeaks corresponding to the DBV and MBV pigments. Therefore, quantum coherence has been proposed to be present for more than 400 fs at physiological conditions. Surprisingly, this effect is active not only between the two coupled DBV superposition states but also between the weakly coupled DBV and MBV bilins. An energy separation of 600 cm^{-1} was found between the two energy levels ascribed to the DBV dimer absorbing at 567 and 588 nm. The absorption of the MBV species was found to be 400 cm^{-1} red-shifted from the lower DBV exciton (at 602 nm), i.e., blue-shifted as compared with the results of Mirkovic et al. (20).

Huo and Coker (22) recently modeled EET and coherence in the first 0.5 ps using the coupling values of Collini et al. (21) and the site energies of Mirkovic et al. (20). Starting from a coherent superposition of excited DBV bilins, excitation was shown to preferentially flow through the MBV B-PCB 158 D side of the complex. At 0.5 ps, ~70% of excitation was still localized on the DBV pair and the rest mainly populated MBV B (12%), PCB 158D (5%), and MBV A (5%). The calculation upon excitation of a single MBV leads to fast depopulation of the MBV (40–30% of excitation is left in 0.3–0.5 ps) mainly to the closest PCB 158 (cf. Fig. 1), meaning that the two MBV bilins do not exchange excitation. At odds with the slow tens-of-picoseconds energy hop between the PCB 82 states found by Mirkovic et al. (20), these two red states form a resonantly coupled dimer that is able to quickly delocalize excitation on both sites of the complex.

The modeling-based study on the PE545 protein complex (23) is also important in relation to PC645 because the two species display a high structural homology (11). In that particular study (23) spectroscopic data for PE545 were modeled using a modified Redfield approach in combination with an improved CIS/6-31G method (11,24,25). It was found that, although no pigment could be considered uncoupled from the others, delocalization was low (1.1–1.2) as a result of the small amount of coupling compared with the differences in unperturbed site energies. A large (~1000 cm^{-1}) splitting between the central DBV 50/61 exciton levels was proposed to contribute to the 545 nm band. In contrast to Doust et al. (11), this splitting is supposed to originate not from strong coupling but from a large difference in the site energy of the two DBV

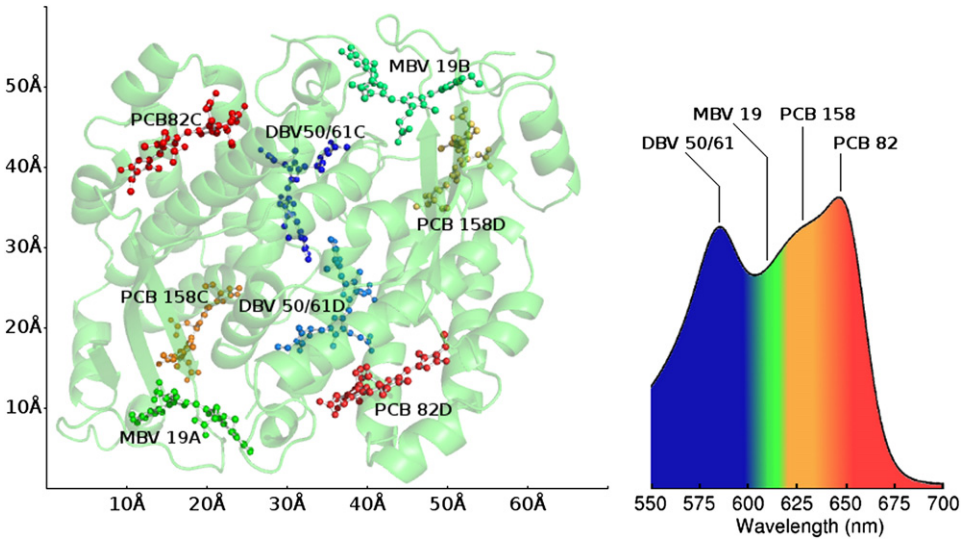

FIGURE 1 Left: Structure of PC645 and labeling of the eight bilin chromophores. Right: Absorption spectrum (see also Fig. 2), indicating the approximate absorption of the bilins.

chromophores. The calculated dynamics in the site representation consist of a 0.18 ps decay of the highest-energy central DBV pigment followed by transfer to the pigments contributing to the 567 nm band in 2–4 ps, and by a final redistribution among the pigments in the red band taking tens of picoseconds.(23)

In this study, we aimed to follow EET in PC645. It is important to provide further spectroscopic evidence for the DBV exciton states, and to verify whether excitation energy of these states simply cascades stepwise down the energy ladder to the MBV and PCB 158 bilins (20,22) or, as we propose in this study, the MBV are not populated by the DBV. In addition, we will address the different assignments for the absorption of the MBV pigments (610–622 (20) or 602 nm (21)), and the discrepancy between calculations and experiments on the lifetime of the final equilibration between the PCB 82 bilins (20).

We performed extensive multicolor pump-probe measurements on isolated PC645 antennae at room and cryogenic temperatures. To assign specific components to EET processes between the bilins, we made use of simultaneous global analysis.

MATERIALS AND METHODS

Sample preparation

PC645 was isolated from *Chroomonas* CCMP270 as explained by van der Weij-de Wit et al. (4). For experiments at cryogenic temperatures, the PC645 preparation was diluted in a solution of 60% glycerol and Hepes (10 mM, pH 7.5) and placed in a 1-mm path cuvette inside an Oxford OptistatDN nitrogen bath cryostat for rapid freezing to 77 K. Glycerol denatures PC645 within several minutes; therefore, the preparation was quickly frozen to 77 K.

Pump-probe setup

Pump-probe experiments were carried out on two different setups. Low-temperature measurements with a pump beam tuned at 585, 633, and 650 nm (see Fig. 4) were recorded in a 1-kHz system as described previously (26). For these experiments, the intensity of the pump was 4 nJ/pulse. The pump and probe beam diameters were 180 and 95 μm, respectively. By correcting the pump intensity by the ratio of the areas of pump and probe beams, we obtained an effective excitation of 1.1 nJ/pulse or slightly higher depending on the energy distribution on the laser spots. Time-gated spectra were recorded at 256 wavelengths between 520 and 730 nm.

The 77 K data obtained at 565 and 601 nm excitation (see Fig. S6 and Fig. S7 in the Supporting Material) and the room temperature (RT) data (see Fig. 3, Fig. S1, Fig. S5, and Fig. S11) were measured in a Mira-RegA femtosecond laser system. Pulses were produced by a titanium:sapphire laser oscillator (MIRA seed; Coherent, Santa Clara, CA) and subsequently amplified by a regenerative amplifier (RegA 9058; Coherent). The output beam was split into two branches: one that was focused on a sapphire plate generating a white light continuum (probe beam), and one that was used to feed a noncollinear optical parametric amplifier NOPA (pump beam). The output pulse of the NOPA (OPA 9850; Coherent) was sent to a variable delay line and overlapped with the probe beam at the place of the sample. The probe light was detected by means of a dispersion system and a 15 or 76 diode array detection system with 3.9 or 1.1 nm resolution, respectively. Time-gated spectra were recorded either in five windows of 15 wavelengths (see Fig. 3, Fig. S4, and Fig. S6) or in two windows of 76 wavelengths (Fig. S5, Fig. S7, and Fig. S11).

For the experiments with the pump beam tuned at 582, 625, 648, and 662 nm, we used a pump pulse with ~10 nJ intensity and with a bandwidth of ~10 nm full width at half-maximum determined by interference filters placed after the NOPA. The temporal width (standard deviation) of the beam was ~115 fs at the sample position, and the repetition rate was set to 150 kHz. Except for the data shown in Fig. S11, the polarization of the pump laser beam was set at the magic angle (54.7°) with respect to the probe beam.

Global analysis

All data obtained at a certain temperature were fitted together with the use of a global analysis routine as described previously (27). Briefly, global analysis is an algorithm that fits all of the data with a number of consecutive exponential decays. The result is a number of evolution associated difference spectra (EADS) and decaying lifetimes. Each EADS decays exponentially and is replaced by the next EADS (i.e., the first EADS decays with the first lifetime, the second EADS rises and decays with the first and second lifetimes, respectively, etc.). The first EADS represents the difference spectrum at time zero, and the fastest lifetimes that can be resolved depend on the temporal resolution of the setup (~100 fs, although one can extract lifetimes of $\leq$80 fs by deconvolving the data with the pulse shape in global analysis (28)). The decay associated difference spectra (DADS) in Fig. S8, Fig. S9, and Fig. S10 show the loss or gain in signal with a certain lifetime. The DADS are linear combinations of the EADS, and vice versa. Thus, the lth EADS is a linear combination of the lth and subsequent DADS. In particular, the first EADS, which corresponds to the time zero difference spectrum, is the sum of all DADS. The final EADS is proportional to the final DADS. A mathematical description of the relation between DADS and EADS can be found in van Stokkum et al. (27) and in the Supporting Material of Toh et al. (29). In the interpretation, EADS are most helpful when describing a cascade of energy transfer processes. DADS allow us to zoom in on small differences (e.g., small spectral shifts) and aid in resolving parallel processes.

RESULTS

Absorption spectra

In Fig. 2 we show the steady-state absorption spectra of PC645 at different temperatures. With a decrease in temperature, the spectra show a gradual sharpening and increase in amplitude of the various bands. The maximum absorption wavelength shifts from 646.5 nm at RT to 654 nm at 77 K. A separate band at 634 nm becomes visible at 77 K that was a shoulder in the RT spectrum. At higher energies, the narrowing is accompanied by a blue shift of the band at 585 to 582.5 nm. Below 500 nm, the RT spectrum shows bands at 234, 278, 340, and 370 nm.

The different excitation wavelengths in Figs. 3 and 4 were chosen to sample different bilins. Excitation at 582/585 nm corresponds to the DBV peak in the OD spectra. At these wavelengths, one would expect the DBV bilins to be selectively excited; however, we also detected the MBV and PCB 158 bilins (vide infra). A mixture of MBV and PCB 158 bilins absorbed at 625/633 nm, and the 648/650 nm excitation tuned to the absorption peak at low energies mostly excited the reddest PCB 82 pair.

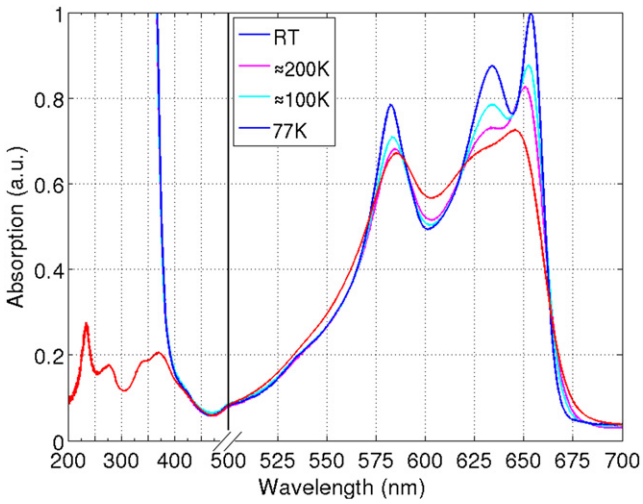

FIGURE 2 Steady-state absorption spectra at different temperatures. The temperatures of the ≈200 K and ≈100 K absorption spectra are indicative. The spectra at low temperatures were normalized on the peak of the 77 K temperature spectrum at 653.7 nm. The RT spectrum was adjusted to the peak of the ≈200 K spectrum at 584.4 nm. The low-temperature spectra are nontransparent below 375 nm due to the absorption of the quartz cuvette (at ~270 and 332 nm) and the glycerol solvent (at 270 nm) used at 77 K.

Global analysis

In this section we describe the results of the RT and 77 K pump-probe on PC645. In Fig. S2 and Fig. S3 typical fits of original pump-probe traces at different excitation and detection wavelengths are plotted.

We used three or four components in the global analysis depending on the dataset. For the datasets with excitation on the red edge (i.e., 648, 650, and 662 nm), three components were sufficient. However, the last two lifetimes of these individual analyses were somewhat variable. The two final lifetimes were estimated in the ranges of 17–55 ps and 0.79–1.38 ns, due to uncertainty in the data. To obtain a better estimate of the two lifetimes, we analyzed all datasets at the same temperature simultaneously and with linking of the last two lifetimes. This model still allows the individual datasets to have components with different spectral shapes. The analysis resulted in two common lifetimes of 44 (46) ps and 1.22 (1.20) ns at RT (77 K). The rationale behind the linking of these two lifetimes is that all excitations should reach the same acceptor pigments via EET. In this case the final state decays with 1.22/1.21 ns, and its precursor decays with ≈44/46 ps.

The estimated lifetimes with and without linking are presented in Table 1 and Table S1, respectively. Linking of the last two lifetimes resulted in only a very small increase in the root mean-square error of the fit (between 0 and 1% for eight of the 10 datasets, the 601 and 662 nm excitation datasets showed a 1.8% and 3.5% increase mainly due to the last approximately nanosecond lifetime). We accept this limitation of the simultaneous analyses to simplify their presentation and interpretation.

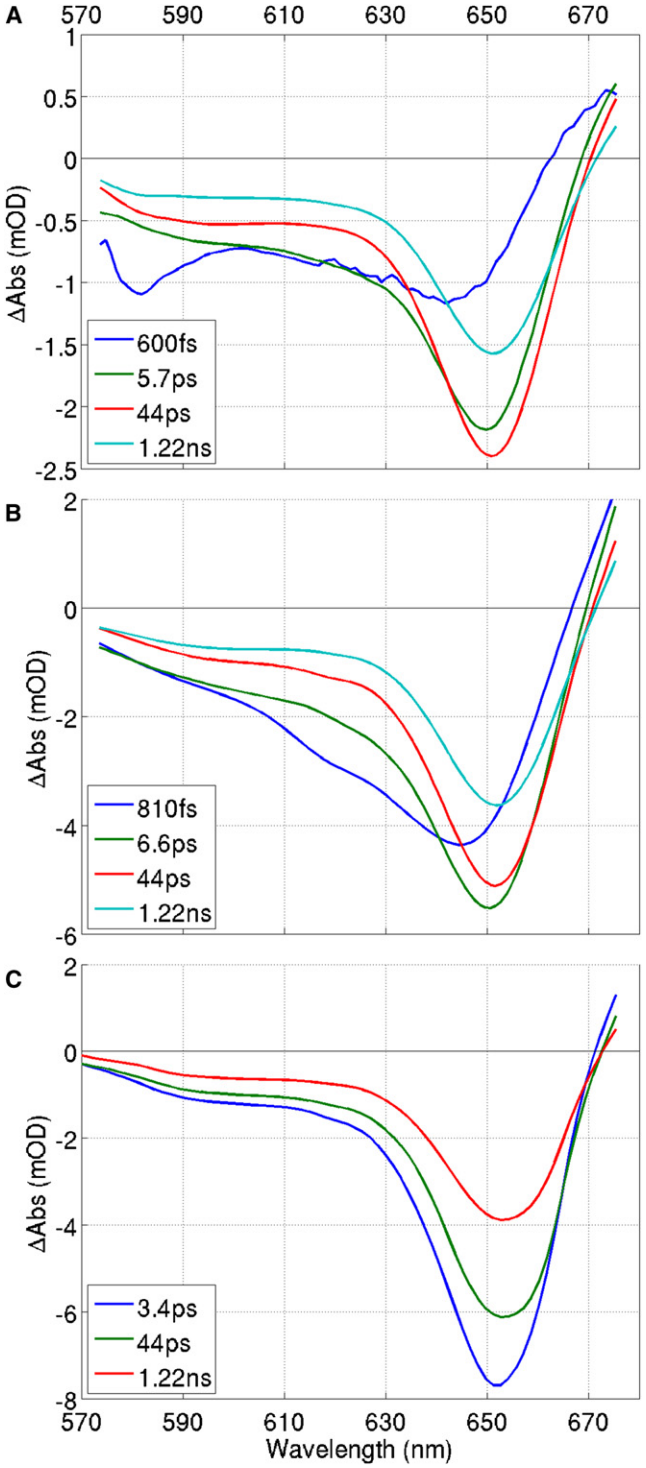

FIGURE 3 EADS from a global analysis of PC645 excited at RT and 582 nm (*A*), 625 nm (*B*), and 650 nm (*C*).

Excitation at 582 nm, RT

The first EADS in Fig. 3 *A* is composed of the bleached absorption of the DBV pair directly excited at 582 nm accompanied by a broad asymmetric bleach between ~610 and

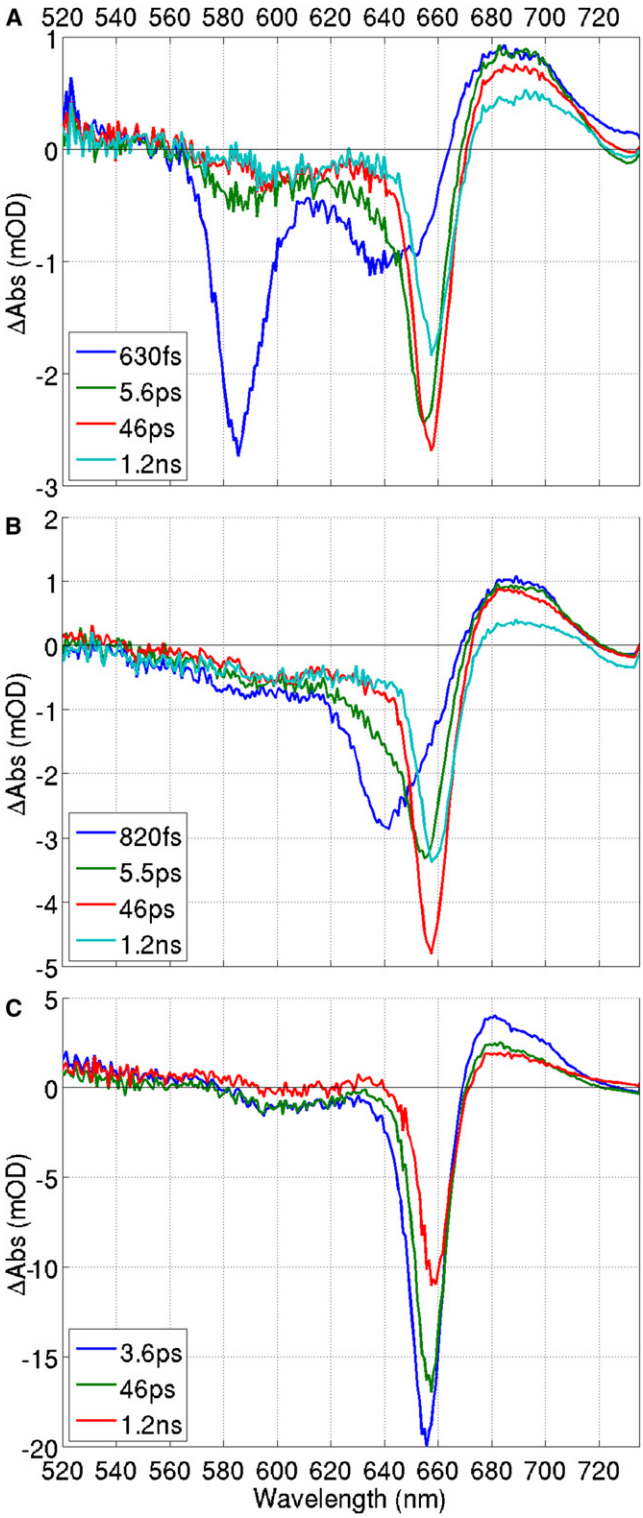

FIGURE 4 EADS from a global analysis of PC645 excited at 77 K and 585 nm (*A*), 633 nm (*B*), and 648 nm (*C*).

663 nm. Excited-state absorption is observed for wavelengths longer than 663 nm. The second EADS shows the complete decay in 0.6 ps of the 582 nm band together with the gain of excitation density between 630 and 674 nm,

TABLE 1 Estimated lifetimes (τ, expressed in ps^{-1}) with linking of the third and fourth lifetimes to 44/46 ps and 1.22/1.21 ns at RT/77 K, respectively

Excitation	Temperature	τ1	τ2	τ3	τ4
400 nm	RT	0.26	2.0	44	1220
582 nm	RT	0.6	5.7	44	1220
625 nm	RT	0.81	6.6	44	1220
648 nm	RT		3.4	44	1220
662 nm	RT	0.7		44	1220
565 nm	77 K	0.95	5.6	46	1210
601 nm	77 K	0.67	6.0	46	1210
585 nm	77 K	0.63	5.6	46	1210
633 nm	77 K	0.82	5.5	46	1210
650 nm	77 K		3.6	46	1210

producing a broad negative band with a peak at 650 nm. No significant change takes place in the spectral region between 600 and 630 nm, where the MBV bilins absorb. At longer wavelengths the isobestic point is shifted to 668 nm, which is caused by the increase in negative contributions to the signal around 650 nm. The third EADS rises in 5.7 ps. The transition shows an overall decrease in the signal below 640 nm concomitant with an increase at slightly lower energies (651 nm). Therefore, the 5.7 ps lifetime describes the complete decay of the bilins with energies in the central (~610–630 nm) part of the spectrum and the population of the red states. The final 44 ps transition shows a small red shift of the bleaching accompanied by an overall decrease in signal. Below 625 nm, the decay shows no spectral features, meaning that excited states at higher energies completely decayed during the previous transitions.

Excitation at 585 nm, 77 K

In the first EADS, a very pronounced initial bleaching appears at 585 nm (Fig. 4 *A*). The spectrum also features a broad bleaching composed of two bands with peaks at 635 and 651 nm, respectively. Above 664 nm, a pronounced excited-state absorption (ESA) band is present, very close to the isobestic point of the first EADS at RT. The 0.63 ps transition shows the decay of the high-energy bilins and the formation of bleaching at 655 nm. Concomitantly, a decay centered at 632 nm takes place (cf. blue DADS in Fig. S8) and the ESA shifts to longer wavelengths (to 669 nm) with no significant change in amplitude. In the next 5.6 ps transition, the bleach narrows due to the loss of excited states below ~650 nm and the ESA shows a 15% drop in amplitude/area. The second DADS (cf. green DADS in Fig. S8) clearly shows that this transition features the decay of a band peaking at 635–650 nm into the PCB 82 at 662 nm, together with a small further decrease around 585 nm. The final spectral evolution takes place in 46 ps and shows a decrease in population of the low-energy states (cf. red DADS in Fig. S8). Although there is no red shift of the absorption peak, a reshaping to lower energies has taken place due to the loss of a bleach at 653–655 nm.

Excitation at 625 nm, RT

The initial bleach/stimulated emission (SE) is composed of a main band at 645 nm and a pronounced shoulder at ~620 nm (Fig. 3 *B*). Clearly, excitation at 625 nm brings about excitation of several bilin species (probably all species except for the DBV pair). The rise in 0.81 ps of the second EADS shows an overall narrowing and red shift of the bleaching to 651 nm. Decaying features are located at ~620 and 630 nm. A second equilibration step takes place in 6.6 ps. Apart from the overall loss of bleaching (20% in the whole wavelength range), the spectral differences between the second and third EADS consist of a small red shift (of ~1 nm) and a narrowing below 650 nm (at ~628 nm). The fourth EADS rises in 44 ps and exhibits a decay of signal centered at 652 nm corresponding to the absorption of the red states. On this timescale, no red shift among the low-energy states is present.

Excitation at 633 nm, 77 K

The first EADS in Fig. 4 *B* initially shows a bleach composed of two bands at ~640 and 650 nm. Similarly to the RT 625 nm dataset, two phases describe the equilibration to the red states: in the faster 0.82 ps transition the decay is centered at 637 nm, whereas in the second 5.5 ps transition it is centered at 643 nm (cf. DADS in Fig. S9). The positive band above 667 nm in the first three EADS shows only minor differences in amplitude and shape, meaning that the different chromophores involved have very similar ESA.

Excitation at 648 nm, RT

The spectra describe the progressive decay of the excited population in the red part of the spectrum (Fig. 3 *C*). The first 3.4 ps evolution shows an additional small red shift from 651 to 653 nm due to intraband equilibration. The last two spectra are identical in shape, showing no further spectral equilibration.

Excitation at 650 nm, 77 K

The 650 nm excitation dataset shows a gradual recovery and red shift of the bleach/SE signal (Fig. 4 *C*). In the first 3.6 ps transition, the decay in bleaching at 651 (cf. blue DADS in Fig. S10) is accompanied by a red shift of the main bleach from 656 to 657 nm. The second transition shows a shift of the bleaching to 659 nm. The ESA around ~680 nm undergoes a decay in proportion with the bleach/SE.

Excitation at 662 nm, RT

We attempted to selectively excite the reddest PCB 82 state of PC645 (Fig. S4). The EADS show a gradual shift in shape to the blue (around 653–654 nm) in 0.7 and 44 ps. No spectroscopic features attributable to DBV or MBV chromophores are present during the two evolutions (cf. DADS in Fig. S10), excluding direct excitation of these pigments.

Excitation at 400 nm, RT

The first EADS includes excited DBV bilins at 584 nm flanked by a negative band up to 660 nm, and a small ESA band peaking at 671 nm (Fig. S5). The first transition shows the formation of a bleaching at 645–650 nm upon decay of the DBV species. The decay of the DBV bilins is completed in the next 2.2 ps transition. This lifetime lies between the 0.8 ps decay found for the DBV species (cf. Fig. 3 *A*) and the slower picosecond dynamics in the 630–670 nm part of the spectrum.

DISCUSSION

In this work we used time-resolved absorption spectroscopy to study the pathways and timescales of EET in the cryptophyte peripheral light-harvesting complex PE645. We selected specific excitation wavelengths to investigate the EET pathway from each bilin species. Excitation at 582/585 nm led to the population of several excited species. We also attempted to extract a faster (<100 fs) initial component in the form of a pure DBV spectrum peaking around 585 nm (result not shown). The result was unsatisfactory; in particular, the spectral shapes and the balance between the areas of the decaying and the product species were not reasonable. Therefore, in this section we present evidence for the DBV exciton states and consider the initial spectra after excitation of the DBV pair to elucidate the different spectral contributions. We then discuss the energy pathway from the species present at time zero. Interestingly, in the central part of the spectrum we find relatively slow picosecond dynamics. Direct excitation of the MBV/PCB 158 pairs at 625/633 nm gives evidence for heterogeneous fast-slow dynamics in the absorption range of the MBV and PCB 158 species. The 650 and 662 nm experiments provide a description of the final EET process between the reddest chromophores, as well as the fluorescence decay time. These experiments confirm that one single species is in the lowest-energy state, despite of the quasi-symmetrical structure of the complex. A time constant of 44/46 ps (RT/77 K) is found for the EET hop between the two reddest PCB 82 bilins.

DBV dimer

The DBV excited-states decay can be considered complete within the subpicosecond lifetime (Figs. 3 *A* and 4 *A*). In our data we cannot find direct evidence for the internal conversion transfer time between the DBV+ and DBV− excitonic states. After excitation of the higher exciton level, one would expect an ultrafast red shift of the SE signal superimposed on the bleach. The magnitude of the red shift

depends on the exact energetic positions of the two states, whereas the rate depends on the spatial overlap of the two excitonic wave functions involved (20,21). Experiments with excitation at 565 nm failed to reveal this phenomenon (cf. Fig. S6); however, the blue-shifted bleaching (at 582 nm compared with 585 in Fig. 4 *A*) suggests that at 565 nm excitation, higher-energy DBV pairs were photoselected. Although Malak and MacColl (18) hypothesized that the excitonic relaxation process could take place in 2 ps, a more realistic estimate would be on the order of <100 fs (vide infra) (30).

The presence of DBV excitonic states was confirmed in the polarized pump-probe experiments shown in Fig. S11. This figure shows the parallel and perpendicular pump-probe traces, together with the calculated anisotropy, after excitation on the blue (578 nm) and red (590 nm) sides of the DBV absorption. We observe that the anisotropy has a different sign at the two excitations, i.e., the amplitudes of the parallel traces are bigger than the perpendicular ones after 590 nm but not after 578 nm excitation. This means that after 578 nm excitation, an ultrafast transition takes place involving strong depolarization and rotation in the orientation of the dipole moment. This rotation is the result of exciton relaxation DBV+ to DBV− when the upper one, DBV+, is photoselected at 578 nm excitation. Exciton relaxation is unresolved with our temporal resolution because the negative anisotropy in the 578 nm excitation traces is instantaneous in our data. Because we are able to extract lifetimes of 80 fs (28), we consider this value as an upper estimate for this relaxation process.

The DBV, MBV, and PCB 158 pairs are excited at 585 nm

Excitation of the DBV bilins at 582/585 nm at both temperatures leads to population of similar bands in the 630–650 nm range (first EADS in Figs. 3 *A* and 4 *A*). These bands contain excited PCB 158 pigments, which were found to absorb around 630 nm (20,21). The 582 nm experiment at RT likely includes contributions from the MBV species, which in the 625 nm experiment (Fig. 3 *B*) are resolved at 620 and 628–630 nm. At 77 K, decaying features (0.63 ps) in the MBV region are present around 635 nm (between 625 and 645 nm). Such features are clearly visible in, e.g., the first DADS of Fig. S8 and Fig. S9. Therefore, it seems that at both RT and 77 K, excited MBV are present with a signal above 618 and 625 nm, respectively.

On the other hand, the first EADS at different temperatures (Figs. 3 *A* and 4 *A*) are quite different in the 600–630 nm range, with a pronounced dip in bleaching/SE in this region of the 77 K data. The greater amount of broadening at RT certainly has a role in this difference. We carried out separate experiments with excitation at 601 and 621 nm (the experiment at 621 nm is not shown) to investigate the possibility that excitation at 633 nm is tuned too much to the red to excite the MBV species at 600–635 nm. The results after 601 nm excitation (Fig. S7) do not indicate any additional band between the DBV and ~620 nm; in general, for the 601 nm experiment, the shape below 630 nm of the first and second EADS are similar to the 633 nm dataset.

In the 585 nm dataset, the species appearing in the central part of the spectrum (in the 620–644 nm range) can be collectively associated with the band in the same spectral range of the 77 K steady-state absorption spectrum (cf. Fig. 2). As noted in the Introduction, the absorption of the MBV species at RT was assigned to 610–622 nm (20) or 602 nm (21). In Fig. 2 it appears that with a decrease in temperature, the 585 nm band in the OD spectrum progressively shifts to lower energies (582 nm), and the shoulder at 621 nm fades away to contribute to the central band at 634 nm. In the 77 K spectrum the difference in width between the central 634 nm and the low-energy (654 nm) bands suggests that the former is composed of more species (e.g., of both MBV and PCB 158). Therefore, the absorption of MBV and PCB 158 at 77 K seems to congest the 620–650 nm spectral range.

In conclusion, we propose that the first EADS after DBV excitation are composed of a superposition of DBV states at 582–585 nm, of MBV at ~618–630/635 nm, and of PCB 158 species at ~642/650 nm at RT/77 K. We explain the spectral differences in the 600–630 nm range between RT and 77 K by band narrowing taking place with decreasing temperature, in combination with a certain degree of red shifting of the MBV absorption.

The first EADS in the 400 nm experiment (Fig. S5) shows a clear DBV spectrum with a smaller contribution from species at lower energies (~640 nm) than after 582 nm excitation. However, the shape of the EADS above ~610 nm suggests that bilins other than the DBVs contribute to the spectrum. Therefore, it seems that also at 400 nm it is not possible to obtain a pure DBV spectrum, because MBV and possibly PCB 158 bilins are also excited. This could be due to the fact that at 400 nm, two bands (a peak at 370 nm and a shoulder at 415 nm; cf. OD spectrum in Fig. 2) contribute to the pump absorption.

The origin of the MBV and PCB 158 excited states in the first EADS after the 582/585 nm excitation is most probably direct excitation of vibronic sidebands. In fact, the MBV/PCB 158 species in the first spectrum after 633 nm excitation (Fig. 4 *B*) presents appreciable background absorption at 585 nm. Shifting the excitation even further to the blue (to 565 nm; see Fig. S6), where the pump absorption of the MBV pair is even smaller, resulted in similar MBV/PCB 158 bands, meaning that excitation of MBV/PCB 158 is also unavoidable in that region.

Alternatively, it is possible that a large fraction of the MBV/PCB 158 band is populated via ultrafast (<100 fs) EET from the DBV. However, we consider this to be unrealistic in view of the relatively weak couplings involved

(21), which would be more consistent with energy transfer times of ~0.5 ps. Furthermore, if that were the case, it would be difficult to explain why the PCB 82 (above 650 nm) are not populated. The DBV bilins are in fact coupled more strongly to both MBV (± 43.9 cm^{-1}) and PCB 82 ($\pm 46.8/48.1$ cm^{-1}) than to PCB 158 (25.3–30.5 cm^{-1}) (21).

Energy pathway from the DBV dimer

The first steps of the energy transfer pathway away from the bilins at high energies are visible in both datasets with excitation at 582–585 nm (Figs. 3 *A* and 4 *A*). The subpicosecond decay time can be assigned to the high-energy DBV pigments, because at 77 K only a negligible fraction of excited DBV pigments seem to be present in the second EADS. This is in very good agreement with the pump-probe traces collected by Mirkovic et al. (20), who reported a 0.62 ps decay at RT after 582 nm excitation, and with the 0.5 ps damping time for the DBV coherent oscillations estimated by Collini et al. (21). The shift of the bleaching to 650/654 nm in 600/630 fs indicates that the PCB 82 species are populated, possibly together with PCB 158. To explain this behavior, we may consider two different mechanisms: either the MBV and the central DBV species transfer independently to the PCB 82, or an additional channel from the DBV via the MBV pigments is active. We observe in the 77 K data that the overall decay above ~610 nm is similar to the 0.82 ps phase in the 633 nm dataset (compare the evolution with the second EADS in the two datasets in Fig. 4, *A* and *B*). Also, the traces at 634 nm after 585 and 633 nm excitation (Fig. S3, *upper* and *lower blue traces*) show an almost identical decay. We therefore suggest that the MBV species undergo an intrinsic subpicosecond decay with no contribution from the DBV. Also, at RT no gain in the MBV region (600–630 nm) is observed. Therefore, we observe direct transfer from the DBV to the PCB states in only 0.6 ps. This conclusion is unexpected given the results of Mirkovic et al. (20) and the earlier observation of electronic coherence involving DBV and MBV (21) that implied EET between these chromophores.

Energy dynamics of MBV and PCB 158 species

After direct excitation in the central part of the spectrum at 625/633 nm excitation (Figs. 3 *B* and 4 *B*), a heterogeneous decay in subpicosecond (0.6–0.8 ps) and picosecond (5–6 ps) phases is found. The 1.12 ps lifetime after 620 nm excitation reported by Mirkovic et al. (20) appears to be an intermediate value in between the two shown in Fig. 4 *B*, and indeed a similar 1.5 ps lifetime is obtained when the 625 nm dataset is fitted with only three components (not shown).

At both 585 and 633 nm excitation, the first decay is blue-shifted as compared with the second (cf. DADS in Fig. S8 and Fig. S9). This suggests that the decay of the MBV species takes place in the first subpicosecond transition, showing a loss at ~632/637 nm. The second 5.5/5.6 ps transition concludes the decay of the central species and describes the relaxation of the redder PCB 158 species.

Similarly, the 625 nm dataset at RT shows a loss at 620–630 nm in 0.81 ps, which includes the absorption range of MBV. The decay in the 6.6 ps transition is now shifted to shorter wavelengths, with a spectral feature at 628 nm. On the other hand, in the 582 nm dataset of Fig. 3 *A*, no evidence is found for a subpicosecond MBV decay, as no change is observed in the MBV range during the first 0.6 ps decay of excited DBV. It is possible that the broader bandwidths at RT obscure the MBV decay. Although we do not have evidence for this, it is probable that excitations preferentially flow along one side of the complex (i.e., through one MBV species), as shown in the models of PC645 (22) and PE545 (23).

The fact that we do not observe EET from MBV to PCB 158 (i.e., no increase in PCB 158 can be seen in the data) leads us to conclude that EET between these chromophores is negligible. This result is somewhat surprising given the calculations of Huo and Coker (22) predicting energy flow through the PCB 158 when the MBV are initially populated.

Final hop between the PCB 82 bilins

By using emission anisotropy and fluorescence anisotropy, Mirkovic et al. (20) provided strong evidence that a single emitter is present in the complex. The final transfer hop was proposed to take place from the PCB 82D to PCB 82C located at the short side of the complex (11,20). We attribute the final 44/46 ps component to this final EET process. Having the lowest-energy states on the smaller sides of the complex is an effective physiological design to ensure efficient transfer between antenna complexes stacked in the intramembrane space (5,6). The lifetimes found for the 648 and 662 nm dataset (see Table S1) are consistent with the study by van der Weij-de Wit et al. (4). In that study, a 45 ps lifetime was found for EET from PC645 to the membrane-associated Chlorophyll *a* containing light-harvesting proteins, whereas a 15–40 ps lifetime was found to govern the final hopping process within PC645 (4). In the study by Mirkovic et al. (20), both the fit for the 645 and 662 nm pump-probe traces and the theoretical results yielded a 36–44 ps lifetime, in agreement with our findings. These authors, however, attributed the slowest 15.5 ps lifetime in the fit of anisotropy with excitation and probing at 662 nm to the final transfer process. The differences between the 648 and 662 nm excitation datasets in our results occur in the spectral equilibration processes: the 648 nm dataset shows in 3.4 ps a small loss of a PCB 82 band at 651 nm (and of PCB 158 at 640 nm), whereas the 662 nm dataset equilibrates in 0.7 ps to the blue. Contrary to what was stated by Mirkovic et al. (20), we find no evidence for excited MVB or PCB

158 species after 662 nm excitation, although this may be due to the narrower pulse width in our experiments. In brief, a final 15 ps hop between the PCB 82 bilins cannot be reconciled with our (and their) pump-probe magic-angle measurements at 645 and 662 nm, both of which indicate a slower lifetime on the order of 40 ps. We note that the anisotropy measurements of Mirkovic et al. were performed up to 100 ps, and the slowest nanosecond component of the fit was replaced with an offset. This might provide a possible explanation for the too fast 15.5 ps component reported in their fit. Moreover, van der Weij-de Wit et al. (4) found a big spread in the estimates of their fluorescence component (15–40 ps).

All of the final transitions consistently show a 33–37% decay of the PCB 82 band area (and amplitude) at RT, and 29–39% at 77 K. In contrast, in the study by van der Weij-de Wit et al. (4), the transition attributed to the final energy transfer step taking place in 15–40 ps shows small fluorescence decay and rise components, implying a negligible loss in fluorescence. Therefore, in the absence of some quenching/annihilation, the only possibility is that the ESA and bleaching in the final spectra overlap differently, leading to compensating contributions in the final spectra.

Model for energy dynamics

The EET dynamics present in the data at 77 K are summarized schematically in Fig. 5. Excitation at 582 nm leads to population of the DBV and to some extent the MBV and PCB 158 bilins. The high-energy DBV pair dissipates the absorbed excitations in 630 fs to the PCB 158 and PCB 82 pairs. Electronic couplings between bilins were reported by Collini et al. (21). For the DBV bilins, the interunit (e.g., DBV 50/61C-PCB 158C) and intraunit (e.g., DBV 50/61C-PCB 158D) couplings are in the same range (20.3–29.0 and 25.3–30.5 cm^{-1}, respectively). Therefore, the intraunit transfer with slightly stronger couplings can hardly be more favorable than the interunit one. More probably, energy is transferred to both PCB 158 species in similar amounts. No energy pathway was detected from the central DBV pigments to the MBV, which is surprising given the finding of coherence between these states (21). In turn, the MBV pair, when directly excited, decays in 0.8 ps to the lowest-energy bilins (PCB 82) but not to the PCB 156 ones. Within 5.6 ps the excitation is equilibrated on the PCB 82 pair absorbing at 651 nm. The final energy transfer process is the 46 ps transfer from the PCB 82 pair.

The energy pathway likely assumes a more asymmetric structure, similar to what was found in the PC645 (22) and PE545 (23) models. In particular, excitation on the central pair in PE545 was shown to favor the population of one side of the complex. In PC645, it is likely that the DBV central pair shows the same behavior, because the coupling between the two central DBV bilins is strongest.

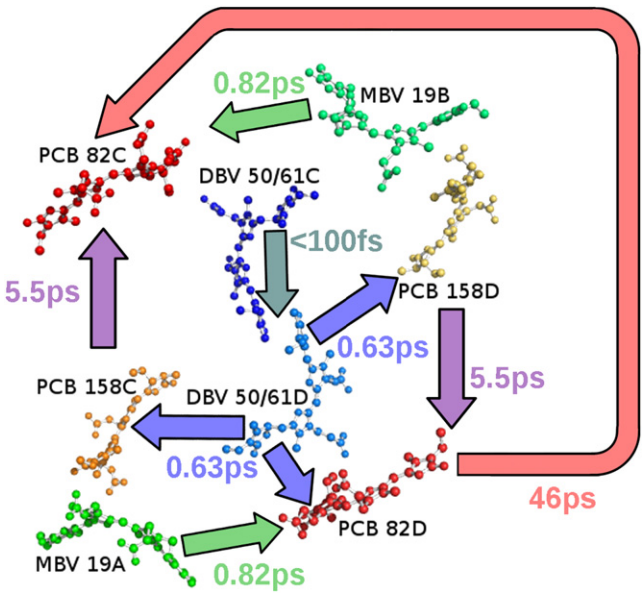

FIGURE 5 Model for energy transfer in PC645. The energy pathways (*arrows*) with corresponding lifetimes (*bold text*) at RT are indicated on the crystal structure of PC645 (see Discussion).

SUPPORTING MATERIAL

A table and 11 figures are available at http://www.biophysj.org/biophysj/supplemental/S0006-3495(11)00842-3.

We thank Jos Thieme for technical support, and Elisabetta Collini for scientific discussion.

This work was supported by the Netherlands Organization for Scientific Research–Chemical Sciences through a TOP grant to R.v.G.

REFERENCES

1. Archibald, J. M., and P. J. Keeling. 2002. Recycled plastids: a 'green movement' in eukaryotic evolution. *Trends Genet.* 18:577–584.
2. Bhattacharya, D., H. S. Yoon, and J. D. Hackett. 2004. Photosynthetic eukaryotes unite: endosymbiosis connects the dots. *Bioessays.* 26:50–60.
3. Gould, S. B., R. F. Waller, and G. I. McFadden. 2008. Plastid evolution. *Annu. Rev. Plant Biol.* 59:491–517.
4. van der Weij-de Wit, C. D., A. B. Doust, …, R. van Grondelle. 2008. Phycocyanin sensitizes both photosystem I and photosystem II in cryptophyte *Chroomonas* CCMP270 cells. *Biophys. J.* 94:2423–2433.
5. Gantt, E., M. R. Edwards, and L. Provasoli. 1971. Chloroplast structure of the cryptophyceae. Evidence for phycobiliproteins within intrathylakoidal spaces. *J. Cell Biol.* 48:280–290.
6. Vesk, M., D. Dwarte, …, R. G. Hiller. 1992. Freeze fracture immunocytochemistry of light-harvesting pigment complexes in a cryptophyte. *Photoplasma.* 70:166–170.
7. Mörschel, E., and W. Wehrmeyer. 1975. Cryptomonad biliprotein: phycocyanin–645 from a *Chroomonas* species. *Arch. Microbiol.* 105:153–158.
8. Wilk, K. E., S. J. Harrop, …, P. M. Curmi. 1999. Evolution of a light-harvesting protein by addition of new subunits and rearrangement of

conserved elements: crystal structure of a cryptophyte phycoerythrin at 1.63-Å resolution. *Proc. Natl. Acad. Sci. USA.* 96:8901–8906.

9. Glazer, A. N., and G. J. Wedemayer. 1995. Cryptomonad biliproteins—an evolutionary perspective. *Photosynth. Res.* 46:93–105.
10. Doust, A. B., C. N. J. Marai, …, G. D. Scholes. 2004. Developing a structure-function model for the cryptophyte phycoerythrin 545 using ultrahigh resolution crystallography and ultrafast laser spectroscopy. *J. Mol. Biol.* 344:135–153.
11. Doust, A. B., K. E. Wilk, …, G. D. Scholes. 2006. The photophysics of cryptophyte light-harvesting. *J. Photochem. Photobiol. A-Chem.* 184:1–17.
12. Hill, D. R. A., and K. S. Rowan. 1989. The biliproteins of the cryptophyceae. *Phycologia.* 28:455–463.
13. Teale, F. W., and R. E. Dale. 1970. Isolation and spectral characterization of phycobiliproteins. *Biochem. J.* 116:161–169.
14. Dale, R. E., and F. W. Teale. 1970. Number and distribution of chromophore types in native phycobiliproteins. *Photochem. Photobiol.* 12:99–117.
15. Kobayashi, T., E. O. Degenkolb, …, D. S. Berns. 1979. Energy transfer among the chromophores in phycocyanins measured by picosecond kinetics. *Biochemistry.* 18:5073–5078.
16. Holzwarth, A. R., J. Wendler, and W. Wehrmeyer. 1983. Studies on chromophore coupling in isolated phycobiliproteins. 1. Picosecond fluorescence kinetics of energy-transfer in phycocyanin–645 from *Chroomonas* sp. *Biochim. Biophys. Acta.* 724:388–395.
17. Jung, J., P. S. Song, …, E. E. Hazen, Jr. 1980. Molecular topography of the phycocyanin photoreceptor from *Chroomonas* species. *Biochemistry.* 19:24–32.
18. Malak, H., and R. MacColl. 1991. A picosecond time-resolved fluorescence study on the biliprotein, phycocyanin 645. *Biochim. Biophys. Acta.* 1059:165–170.
19. Csatorday, K., D. Guard-Friar, …, D. S. Berns. 1988. The development of exciton migration routes for phycocyanin 645 and allophycocyanin. *Photochem. Photobiol.* 47:285–291.
20. Mirkovic, T., A. B. Doust, …, G. D. Scholes. 2007. Ultrafast light harvesting dynamics in the cryptophyte phycocyanin 645. *Photochem. Photobiol. Sci.* 6:964–975.
21. Collini, E., C. Y. Wong, …, G. D. Scholes. 2010. Coherently wired light-harvesting in photosynthetic marine algae at ambient temperature. *Nature.* 463:644–647.
22. Huo, P., and D. F. Coker. 2011. Theoretical study of coherent excitation energy transfer in cryptophyte phycocyanin 645 at physiological temperature. *J. Phys. Chem. Lett.* 2:825–833.
23. Novoderezhkin, V. I., A. B. Doust, …, R. van Grondelle. 2010. Excitation dynamics in phycoerythrin 545: modeling of steady-state spectra and transient absorption with modified Redfield theory. *Biophys. J.* 99:344–352.
24. Scholes, G. D., C. Curutchet, …, J. Tomasi. 2007. How solvent controls electronic energy transfer and light harvesting. *J. Phys. Chem. B.* 111:6978–6982.
25. Curutchet, C., G. D. Scholes, …, R. Cammi. 2007. How solvent controls electronic energy transfer and light harvesting: toward a quantum-mechanical description of reaction field and screening effects. *J. Phys. Chem. B.* 111:13253–13265.
26. Marin, A., F. Passarini, …, R. van Grondelle. 2010. Energy transfer pathways in the CP24 and CP26 antenna complexes of higher plant photosystem II: a comparative study. *Biophys. J.* 99:4056–4065.
27. van Stokkum, I. H. M., D. S. Larsen, and R. van Grondelle. 2004. Global and target analysis of time-resolved spectra. *Biochim. Biophys. Acta.* 1657:82–104.
28. Marin, A., F. Passarini, …, R. Croce. 2011. Minor complexes at work: light-harvesting by carotenoids in the photosystem II antenna complexes CP24 and CP26. *Biophys. J.* 100:2829–2838.
29. Toh, K. C., E. A. Stojković, …, J. T. Kennis. 2010. Proton-transfer and hydrogen-bond interactions determine fluorescence quantum yield and photochemical efficiency of bacteriophytochrome. *Proc. Natl. Acad. Sci. USA.* 107:9170–9175.
30. van Grondelle, R., and V. I. Novoderezhkin. 2006. Energy transfer in photosynthesis: experimental insights and quantitative models. *Phys. Chem. Chem. Phys.* 8:793–807.